2D & 3D numerical analyses of a deep excavation supported by LC columns

Citation for the original published paper (version of record):
Bozkurt, S., Abed, A., Karstunen, M. (2023). 2D & 3D numerical analyses of a deep excavation supported by LC columns. 10th European Conference on Numerical Methods in Geotechnical Engineering Zdravkovic L, Kontoe S, Taborda DMG, Tsiampousi A (eds): 1-6.
http://dx.doi.org/10.53243/NUMGE2023-188

Proceedings 10th NUMGE 2023
10th European Conference on Numerical Methods in Geotechnical Engineering
Zdravkovic L, Kontoe S, Taborda DMG, Tsiampousi A (eds)

https://doi.org/10.53243/NUMGE2023-188

2D & 3D numerical analyses of a deep excavation supported by LC columns

S. Bozkurt[1], A. Abed[1], M. Karstunen[1]

[1] *Architecture and Civil Engineering, Chalmers University of Technology, Gothenburg, Sweden*

ABSTRACT: This paper presents finite element simulations of an instrumented deep excavation in soft clay. The excavation is supported with sheet pile walls utilising lime-cement (LC) columns in the passive side. The measured deformations were back-calculated using a two-dimensional (2D) plane strain model, as well as a full three-dimensional (3D) model, in conjunction with fully coupled consolidation analysis. Prescribed volumetric strain was used to capture the installation effects of the LC columns. Advanced constitutive models were utilised for both the natural and stabilised clay. The model parameters used to simulate LC columns were derived and calibrated using triaxial extension tests. The 2D analysis was performed using a simple stiffness averaging technique, whereas in the 3D analysis the columns and the soil were modelled separately. The displacement profile captured by the inclinometer located at the intersection with the nearby excavation site could be captured only with the 3D analysis. The numerical results of both the 2D and the 3D analyses indicate that the inclusion of installation effects was crucial to replicate the field response.

Keywords: excavation; deep mixing; lime-cement; soft soil; ground improvement

1 INTRODUCTION

Ground improvement with deep mixing methods has widely been used since the late 1960s. The use of deep mixing for braced excavations in soft soils increases the stability against basal heave and reduces lateral deformations towards the excavation. Furthermore, it eases the excavation process itself. Typically in excavations, overlapping deep-mixed columns are applied, using either dry (Ignat et al., 2020) or wet mixing methods (O'Rourke & O'Donnell, 1997; Tanaka, 1993). In dry mixing process, binders undergo hydration with the water already present in the natural soil (Larsson, 2017). In Sweden, the dry mixing method is most often executed using quicklime (unslaked lime) and Portland cement.

The use of deep soil mixing in excavations changes the initial stress state. Even though overall response due to excavation is dominated by the soft soil, the field performance is affected by various factors associated with the column installation: 1) soil disturbance by the mixing procedure (the use of compressed air, admixture injection and shearing due to blade rotation), 2) thixotropy and soil fracturing arising from soil disturbance, geotechnical properties *in situ* and the inclusion of admixtures, 3) chemical reactions and ion exchange within stabilised soil, and 4) consolidation (Shen et al., 2008).

Current guidelines (e.g., Bruce et al., 2013; EN14679, 2005; EuroSoilStab, 2002) on the deep mixing design propose simple rigid-plastic solutions based on methodologies described in Broms & Boman (1979) with focus on the application under embankments. These guidelines suggest empirical relationships between the undrained shear strength (measured from vane, UC, fall-cone, plate load, static penetration tests, etc.) and the stiffness. Ergo linear elastic or linear elastic-perfectly plastic assumptions are used to model the behaviour of deep mixed columns. However, using elastic models, in general does not represent adequately the real behaviour of soils (Jardine et al., 1986).

This study investigates stress-strain response of a deep excavation supported by lime-cement columns. The use of advanced soil models, for both *in situ* and stabilised clay, and considering installation effects, enables realistic deformation calculations using 2D and 3D analyses.

2 SITE LOCATION AND GEOTECHNICAL CONDITIONS

The instrumented excavation in question is a part of the West Link railway construction project, which consists of a six-kilometre railway tunnel underneath the centre of Gothenburg. A 200-m long temporary excavation tunnel section (Km: 456+850, E02 Central Station) was monitored via inclinometers for a construction period of 8 months. The braced excavation was supported by sheet pile walls (SPW), waler beams, two levels of struts and overlapping lime-cement (LC) columns in the

passive side (Figure 1). In order to facilitate an economic design, different lime-cement ratios were utilised above and below the excavation, 40 kg/m^3 and 80 kg/m^3, respectively.

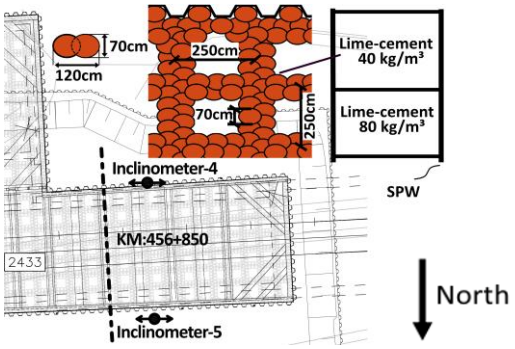

Figure 1. Location of the inclinometers and cross-section of E02 Central station of West Link deep excavation.

The soft clay deposit is geologically young with an overconsolidation ratio (OCR) in the range of 1.00 to 1.50. Ground water is located about 2 m below the ground surface. The total depth of the medium sensitive, high plastic, glacial-post glacial soft clay is as deep as 55-75 m in the area considered. The natural clay has consolidated under its own weight due to mainly one-dimensional deposition, followed by fill materials on top, and therefore considerable background creep deformations are expected. Furthermore, the soil exhibits significant initial anisotropy.

3 NUMERICAL MODELLING OF THE EXCAVATION

The construction stages of the 11 m deep excavation were monitored via two inclinometers (Figure 1). Before SPW and LC column installation, 2 m of fill was excavated. After this excavation, SPWs were installed. Later on, in the passive side of the excavation, lime-cement columns with diameters of 0.7 m were constructed in a square grid, with 2.5 m spacing and 0.2 m overlap.

The installation of deep mixed columns creates considerable deformations which can be evaluated by using field monitoring data (O'Rourke & O'Donnell, 1997). The effect of column installation can be taken into account by subjecting the stabilised soil to radial strain before the external loads are applied (Schweiger & Pande, 1988). In the numerical analyses, the mixing-related deformations were simulated in the back-analyses by the application of an external prescribed strain. The prescribed strains were calibrated with the aid of inclinometer measurements throughout the column installation phase. The external strains were applied in both radial axes in order to obtain the same displacement profile as the field measurements.

The nature of the braced excavation involves three-dimensional effects. In many cases, it is not feasible to perform 3D analyses. Thus, the true geometry of the soil-column system and the 3D effects are often simplified. However, 3D and plane strain simulations of excavations may not yield the same displacement profile (Finno et al., 2007). Therefore, in this study, a 2D analysis as well as a 3D analysis were performed in conjunction with fully coupled consolidation analysis (PLAXIS 2D & 3D version 22). To reduce the effect of discretisation, comparable meshes were utilised in the 2D and the 3D analyses with 1537 elements and 3242 nodes, and 31290 elements and 49281 nodes, respectively, as shown in Figure 2.

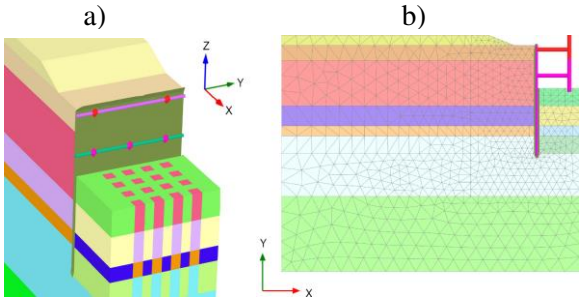

Figure 2. The used FE model in (a) 3D and (b) 2D analysis.

3.1 Modelling of soft soil with Creep-SCLAY1S

The soft clay was represented by the Creep-SCLAY1S model (Gras et al., 2018; Sivasithamparam et al., 2015) which describes fundamental features of natural soft soils, such as rate dependency, anisotropy and destructuration, accounting for changes in fabric and interparticle bonding. The model incorporates normal consolidation surface (NCS) representing the outer boundary between large and small creep strains. This bounding surface (f_{NCS}) can be expressed with Equation (1) in triaxial stress space.

$$f_{NCS} = (q - \alpha p')^2 - (M(\theta)^2 - \alpha^2)(p'_p - p')p' \quad (1)$$

where $q = (\sigma'_1 - \sigma'_3)$ is the deviator stress and $p' = (\sigma'_1 + \sigma'_2 + \sigma'_3)/3$ is the mean effective stress. p'_p defines the size of NCS, while α defines the orientation of NCS. $M(\theta)$ is the Lode angle dependent stress ratio at critical state ($M = q/p'$ with $m = M_c/M_e$) (Equation (2)).

$$M(\theta) = M_c \left(\frac{2m^4}{1+m^4+(1-m^4)\sin 3\theta_\alpha}\right)^{1/4} \quad (2)$$

M is calculated at critical state in triaxial compression (TXC), isochoric shear (SHR) and triaxial extension (TXE) for θ_α= -30°, θ_α= 0° and θ_α= +30°, respectively. The function of the second and third deviatoric stress invariants defines θ_α (Sheng et al., 2000). Creep-SCLAY1S determines the changes in the sheared ellipse in terms of size, rotation, and progressive loss of bonding with volumetric and deviatoric creep straining. In addition to NCS, the model incorporates other two loci,

namely the current stress surface (CSS) and the intrinsic compression surface (ICS), which define the current state of effective stress (p'_{eq}) and the imaginary surface with all bonding destroyed. For detailed mathematical formulation of the model, and its 3D formulation used in the FE simulations, the reader is referred to (Gras et al., 2018; Sivasithamparam et al., 2015).

Creep-SCLAY1S parameters (Tables 1 and 3) were calculated from laboratory tests (CADC/E and CAUC/E, CRS and IL) and calibrated using Plaxis SoilTest facility. The selected values for the modified intrinsic compression index, λ_i^*; modified swelling index, κ^*; Poisson's ratio, ν'; critical state stress ratio in compression and extension, M_c and M_e; absolute and relative effectiveness of rotational hardening, ω and ω_d respectively; absolute rate of destructuration, a ; relative rate of destructuration due to deviator strain, b ; initial anisotropy, α_0; initial void ratio, e_0 are listed in Table 3. The preconsolidation ratio of the soil was calculated using IL and CRS data (Table 1). POP is defined as the difference between the preconsolidation pressure and the vertical effective stress. The values correspond to reference time τ of 1 day.

Table 1. Initial soil parameters for the soft clay.

Layer	*POP*	e_o	c_k	k_h=k_v *(m/day)*
Clay fill	30	1.91	0.95	0.56x10^{-4}
Layer-1	30	2.24	0.44	1.30x10^{-4}
Layer-2	25	1.97	0.24	0.63x10^{-4}
Layer-3	20	1.90	0.27	0.75x10^{-4}
Layer-4	15	1.83	0.30	0.86x10^{-4}
Layer-5	0	1.69	0.29	0.52x10^{-4}

Table 2. Parameters of the fill layer.

Layer	γ_n *(kN/m^3)*	E' *(kPa)*	c' *(kPa)*	ϕ' (°)	ν' *(-)*
Fill	17	20000	5	30	0.25

Table 3. Creep-SCLAY1S parameters for the soft clay.

	Layer-1*	Layer-2	Layer-3	Layer-4	Layer-5
λ_i^*	0.085	0.080	0.085	0.080	0.085
κ^*	0.006	0.008	0.007	0.005	0.008
ν'			0.20		
M_c	1.45	1.18	1.10	1.12	1.10
M_e	0.97	1.15	0.99	0.99	1.20
ω	20	35	50	50	50
ω_d	0.98	0.74	0.64	0.66	0.70
a	12	12	12	12	12
b	0.2	0.2	0.4	0.2	0.2
μ_i^*			0.006		
χ_0			6		
α_0	0.56	0.45	0.42	0.43	0.44
K_0^{NC}	0.42	0.54	0.54	0.53	0.52

* Clay fill layer has the same parameter set, except different permeability and POP (as shown in Table 1).

3.2 Modelling of LC columns with MNhard

The lime-cement columns were simulated with Matsuoka-Nakai hardening (MNhard) soil model (Benz, 2007). The model considers shear hardening and ultimate failure based on Matsuoka-Nakai failure criterion (Matsuoka and Nakai, 1974). The shear hardening of the model was formulated by utilising a nonlinear stress-strain relationship for both primary loading and elastic un-/reloading (Benz, 2007).

The parameters for the stabilised soil were calculated and calibrated using CAUE and IL tests performed on both *in situ* mixed and laboratory mixed samples, as seen in Figure 3. In the 2D analysis, a simple stiffness averaging technique (Broms, 2004) using a theoretical area replacement ratio of 0.66 was employed (Table 4), considering a mixture of clay and LC columns, whereas in the 3D analysis, LC columns were modelled separately (Table 5).

Table 4. MNhard soil model parameters for stabilised area (2D FE analysis).

γ_n *(kN/m^3)*	G_{50}^{ref} *(kPa)*	G_{ur}^{ref} *(kPa)*	p^{ref} *(kPa)*	m *(-)*	ϕ' (°)	c' *(kPa)*	ν' *(-)*
17	20000	50000	100	0.65	37	20	0.25

Table 5. MNhard soil model parameters for lime-cement columns (3D FE analysis).

γ_n *(kN/m^3)*	G_{50}^{ref} *(kPa)*	G_{ur}^{ref} *(kPa)*	p^{ref} *(kPa)*	m *(-)*	ϕ' (°)	c' *(kPa)*	ν' *(-)*
17	28000	75000	100	0.65	37	20	0.25

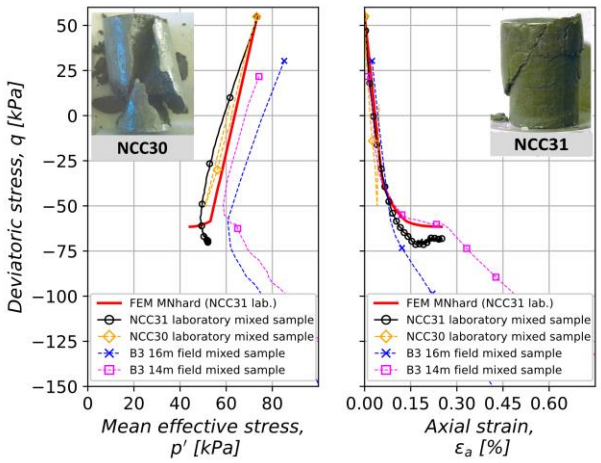

Figure 3. Simulation of CAUE tests on stabilised clay.

4 RESULTS

4.1 Stress-strain response within soft soil

The predicted stress paths in the excavation are shown in the π-plane (Figure 4) for specific locations: inside the active wedge behind the SPW (*Point A, Point B*) and inside the passive wedge (*Point C*) beneath the bottom of the excavation.

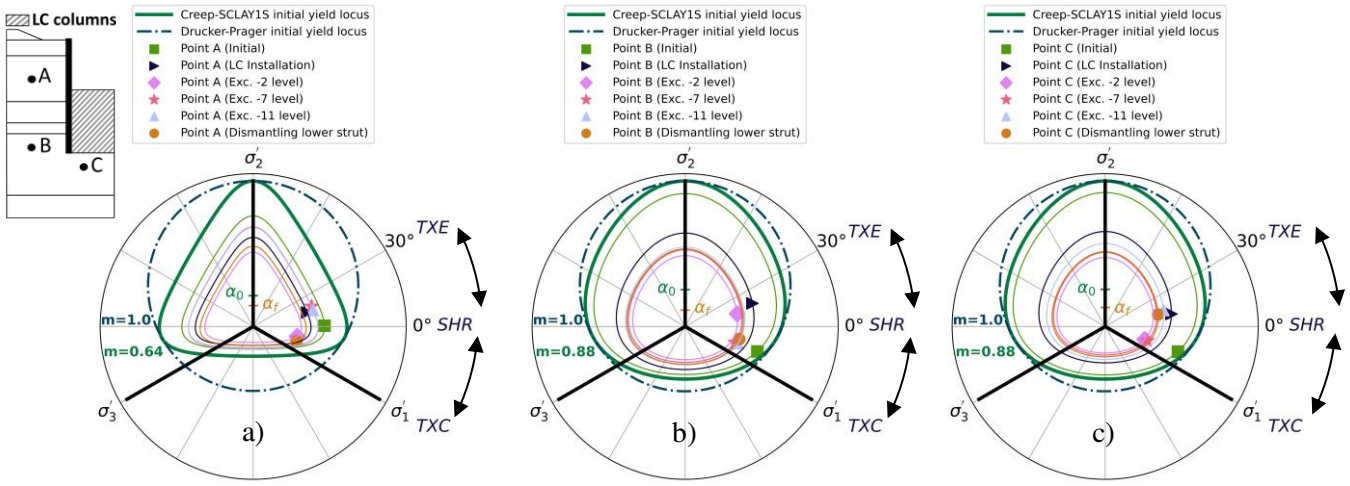

Figure 4. Followed stress path in the π plane from the 2D FE analysis. (a) Point A, (b) Point B and (c) Point C.

NCS adopted by Creep-SCLAY1S indicated significant initial anisotropy (α_0) which was gradually reduced to α_f with volumetric and deviatoric creep straining. Convexity of NCS stems from the layer-dependent m values. The value of m =1 would correspond to a circular Drucker–Prager failure surface.

Prescribed strain application representing the installation effects during the LC column construction stage resulted in extension at all points. The unloading and the wall deformation resulted in either compression or extension, depending on the increments in radial and vertical principal stresses. The increase in radial stresses due to the strut installation was more pronounced for *Point A* than *Point B*. Unloading led to compression state for *Point B,* whereas extension state for *Point C*.

4.2 Deformation predictions

Field deformations were monitored via two inclinometers (*Inc-5* and *Inc-4)* for a construction period of 8 months. According to both measurements, the LC column installation created large horizontal displacements, corresponding to an order of 50 mm behind the wall, indicated by negative values (Figure 5 and Figure 6(a)). These values were far too large to be ignored. The installation effects were simulated by application of a prescribed volumetric strain prior to the main excavation.

The first excavation phases (Figures 6(a) and (b)) of the analyses highlight an analogous deformation profile for the 2D & 3D analyses. Starting from excavation to level -7, however, a noticeable difference between the two predictions can be observed (Figure 6(c)). Large deformations calculated by the 3D analysis at the mid-span corresponded to the measurements of *Inc-4*, whereas these excess deformations were not captured in the 2D analysis and in *Inc-5*. The measurements of the far-field inclinometer, *Inc-5* are not as sensitive as *Inc-4* to the adjacent construction and 3D effects, ergo the north section of the excavation was exposed to a more uniform stress distribution behind the SPW.

The time-dependent lateral deformation profile calculated by the 2D analysis is in accordance with Inc-5 (Figure 5). Lateral deformations away from the excavations indicated by negative values changed the direction to towards excavation with the excavation in progress.

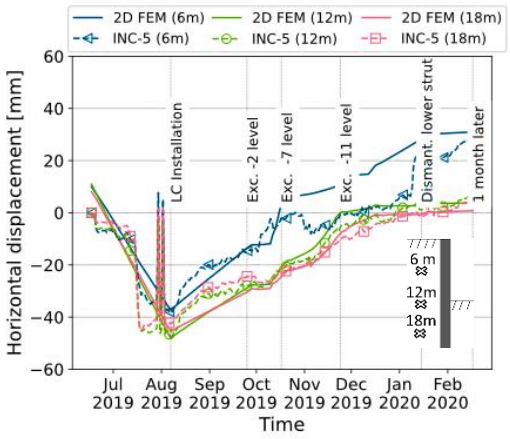

Figure 5. Comparison of horizontal displacements measured and predicted by the 2D FE analysis. Negative values indicate displacements away from the excavation.

Large deformations with the positive values are more pronounced after the excavation to level -7, particularly for the 3D analysis (Figure 7). The excess lateral deformations towards to the excavation deviated from the 2D analysis, and a similar deformation profile measured in Inc-4 was observed. At the end of the excavation, the 3D analysis yielded a higher maximum lateral deformation than that of the 2D analysis, with the order of 2 cm. The 3D analysis resulted with the most unsafe deformation predictions, whereas the 2D analysis resembled a more uniform stress distribution at the north section. The analyses were able to capture reasonably well the deformation response recorded in the field.

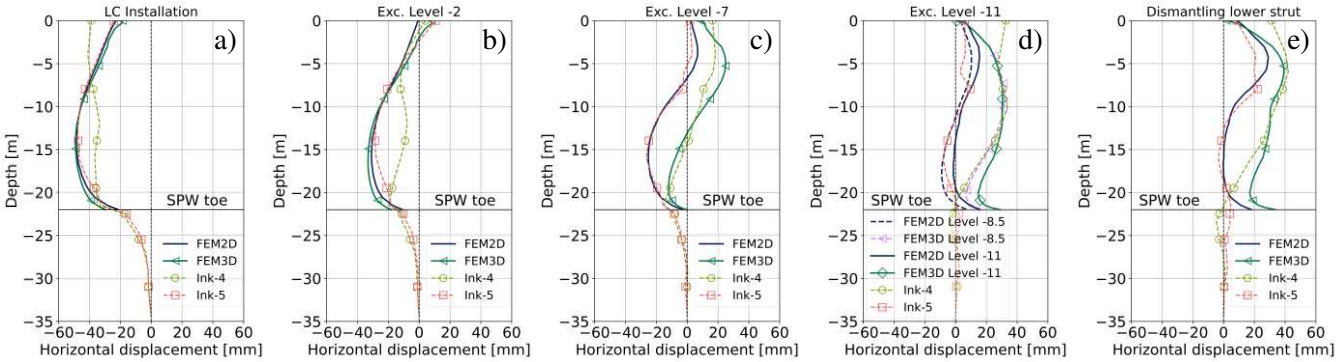

Figure 6. Comparison of horizontal displacements measured and predicted by the 2D & 3D FE analyses. Negative values indicate displacements away from the excavation.

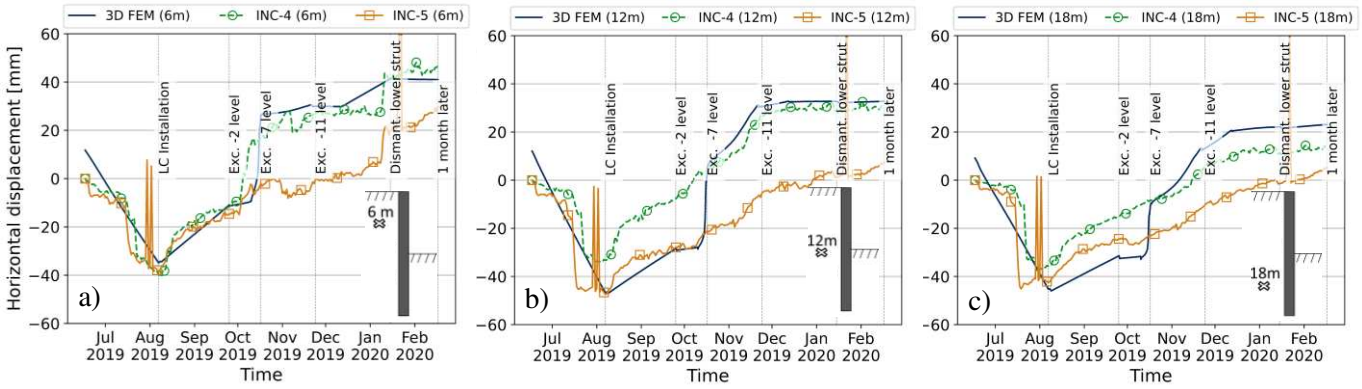

Figure 7. Comparison of the horizontal displacements measured and predicted by the 3D FE analysis. Negative values indicate displacements away from the excavation. Locations of the predictions: (a) 6 m, (b) 12 m and (c) 18 m.

4.3 Strut axial force predictions

In order to measure the distribution of axial forces acting on the struts, strain gauges were mantled on four struts and measurements were made in different locations (Figure 8(b), locations 1, 2, 3 and 4). The upper struts (*Strut 1* and *Strut 2*) were monitored in two sections: the middle of the span and at a distance of 3 m from the end-bearing plates, whereas the lower struts were monitored at a distance of 3 m from the end-bearing plates.

The excavation processes in the nearby excavations, the time differences in the installation of the struts, and the temperature effects caused large variations in the field measurements. Variation in strut spacing caused a higher force distribution in *Strut-1*. Nevertheless, the change in the spacing could not be reflected in the analyses due to the simplifications made in the geometry, which assumed the average values of the strut spacings.

At the upper strut level, the arching effect of the support system resulted in a different loading mechanism between the 2D and the 3D simulations (Figure 9(a)). Therefore, the maximum axial forces calculated by the 3D analysis are smaller than by the 2D analysis. The measurements of *Strut 1* are comparable to the 2D analysis, whereas the measurements of *Strut 2* and the 3D analysis were more similar compared to the 2D analysis.

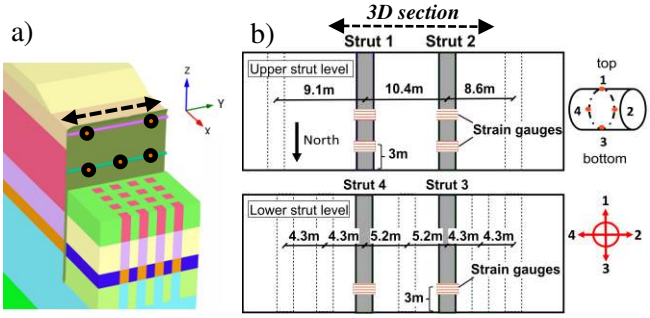

Figure 8. Strut and strain gauge installation locations. (a) the 3D FE analysis, (b) plan view.

Similarly, according to field data, the lower mid-span strut (*Strut 3)* was exposed to a higher force (Figure 9(b)) resulting from the varied spacing of the upper struts. The mid-span stress distribution of the struts cannot be captured by the 2D simulation accurately. However, the results of the plane strain simulation corresponded to the 3D simulation and those of *Strut-3,* as the lower strut spacing was not as variable as the upper struts, and thus the force distribution was more uniform than in the upper struts.

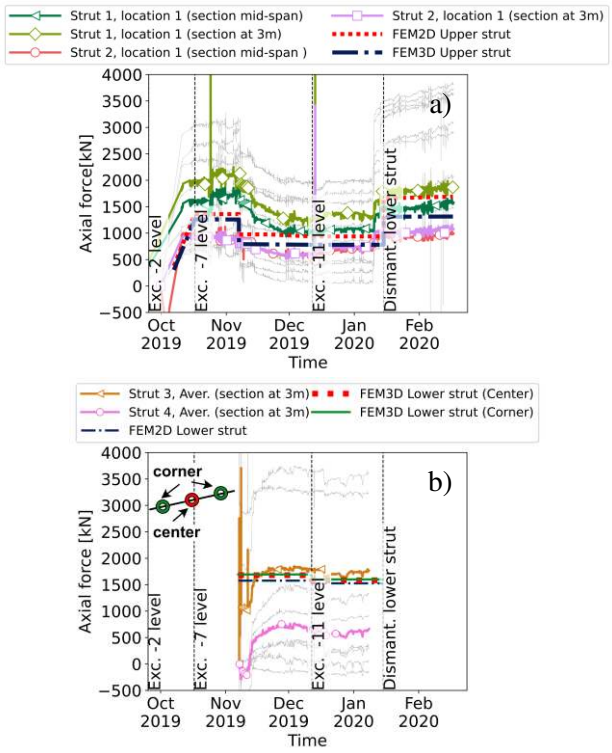

Figure 9. Strut force distribution in the 2D&3D FE analyses: (a) upper strut, (a) lower strut.

5 CONCLUSIONS

2D and 3D numerical analyses of a deep excavation supported by sheet pile walls and lime-cement columns formed using dry mixing method were performed. During the analyses, the mixing-related deformations arising from installation effects were computed with the prescribed strain application. Inclinometers installed in the site provided simultaneous field measurements against which the 2D and 3D analyses predictions were compared and validated. The numerical results indicated that the accurate predictions of the deformations and structural forces necessitate taking into account the installation effects and the three-dimensional effects.

6 ACKNOWLEDGEMENTS

The work is funded by Formas (Research Council for sustainable Development, Grant (2019-00456) and Swedish Transport Administration (Grant 2020/46703) via BIG (Better Interaction in Geotechnics). The work is done as part of Digital Twin Cities Centre that is supported by Sweden's Innovation Agency VINNOVA (Grant 2019-00041). The authors would like to thank Jonatan Isaksson from NCC AB for making the laboratory and field data available for the project.

7 REFERENCES

Benz, T. (2007). Small-Strain Stiffness of Soils and its Numerical Consequences [PhD thesis]. University of Stuttgart, Germany.

Broms, B. B. (2004). Lime and lime/cement columns. *Ground Improvement*, *2*, 252–330.

Broms, B. B., & Boman, P. (1979). Lime Columns—A New Foundation Method. *Journal of the Geotechnical Engineering Division*, *105*(4), 539–556.

Bruce M. E. C., Berg R. R., Collin J. G., Filz G. M, Terashi, M., & Yang D. S. (2013). *Federal Highway Administration Design Manual: Deep Mixing for Embankment and Foundation Support*. Offices of Research and Development, Federal Highway Administration, Washington, DC, USA, Report No. FHWA-HRT-13-046.

EuroSoilStab (2002). Development of design and construction methods to stabilize soft organic soils: Design guide for soft soil stabilization. *CT97-0351, European Commission, Industrial and Materials Technologies Programme (Rite-EuRam III) Bryssel*.

Finno, R. J., Blackburn, J. T., & Roboski, J. F. (2007). Three-dimensional effects for supported excavations in clay. *Journal of Geotechnical and Geoenvironmental Engineering*, 133(1), 30-36.

EN14679 (2005). European Standard, Execution of Special Geotechnical Works – Deep Mixing.

Gras, J. P., Sivasithamparam, N., Karstunen, M., & Dijkstra, J. (2018). Permissible range of model parameters for natural fine-grained materials. *Acta Geotechnica*, *13*(2), 387–398.

Ignat, R., Baker, S., Karstunen, M., Liedberg, S., & Larsson, S. (2020). Numerical analyses of an experimental excavation supported by panels of lime-cement columns. *Computers and Geotechnics*, *118*, 103296.

Jardine, R. J., Potts, D. M., Fourie, A. B., & Burland, J. B. (1986). Studies of the influence of non-linear stress–strain characteristics in soil–structure interaction. *Géotechnique*, *36*(3), 377–396.

Larsson, S. (2017). The mixing process at the dry jet mixing method. In H. Bredenberg (Ed.), In *Dry Mix Methods for Deep Soil Stabilization* (pp. 339–346). Routledge.

Matsuoka, H., & Nakai, T. (1974). Stress-deformation and strength characteristics of soil under three different principal stresses, In *Proceedings of the Japan Society of Civil Engineers* (pp. 59–70).

O'Rourke, T. D., & O'Donnell, C. J. (1997). Field Behavior of Excavation Stabilized by Deep Soil Mixing. *Journal of Geotechnical and Geoenvironmental Engineering*, *123*(6).

Schweiger, H. F., & Pande, G. N. (1988). Numerical analysis of a road embankment constructed in soft clay stabilised with stone columns. *Proceedings of the Sixth International Conference on Numerical Methods in Geomechanics, Innsbruck, 11-15 April*. 1329–1333.

Shen, S. L., Han, J., & Du, Y. J. (2008). Deep Mixing Induced Property Changes in Surrounding Sensitive Marine Clays. *Journal of Geotechnical and Geoenvironmental Engineering*, *134*(6), 845–854.

Sheng, D., Sloan, S., & Yu, H. (2000). Aspects of finite element implementation of critical state models. *Computational Mechanics 26*, 185–196.

Sivasithamparam, N., Karstunen, M., & Bonnier, P. (2015). Modelling creep behaviour of anisotropic soft soils. *Computers and Geotechnics*, *69*, 46–57.

Tanaka, H. (1993). Behavior of Braced Excavations Stabilized by Deep Mixing Method. *Soils and Foundations*, *33*(2), 105–115.